

Revised manuscript 4 January 2020/PSt

1
2
3
4
5
6
7
8
9
10
11
12
13
14
15
16
17
18
19
20
21
22
23
24
25
26
27**The Polar Cap (PC) index: invalid index series and a different approach.**

Peter Stauning

Danish Meteorological Institute, Copenhagen, Denmark

Mail: pst@dmi.dk**Abstract.**

The Polar Cap (PC) indices are derived from the magnetic variations generated by the transpolar convection of magnetospheric plasma and embedded magnetic fields driven by the interaction with the solar wind. The PC indices are potentially very useful for Space Weather monitoring and forecasts and for related research. However, the PC index series in the near-real time and final versions endorsed by the International Association for Geomagnetism and Aeronomy (IAGA) are considered unreliable. Both versions include solar wind sector (SWS) effects in the calculation of the reference levels from which magnetic disturbances are measured. The SWS effects are caused by current systems in the dayside Cusp region related to the Y-component, B_Y , of the Interplanetary Magnetic Field (IMF). However, the IAGA-endorsed handling of SWS effects may generate unfounded PC index changes of up to 3 mV/m at the nightside away from the Cusp. For the real-time PCN and PCS indices, the cubic spline-based reference level construction may cause additional unjustified index excursions of more than 3 mV/m with respect to the corresponding final index values. Noting that PC index values above 2 mV/m indicate geomagnetic storm conditions, such unjustified contributions are considered to invalidate the IAGA-endorsed PC index series. Alternative derivation methods are shown to provide more consistent index reference levels for both final and real-time PC indices, to reduce their unfounded excursions, and to significantly increase their reliability.

28 1. Introduction.

29 The Polar Cap (PC) indices, PCN (North) and PCS (South) are based on magnetic data recorded at
30 the central polar cap observatories in Qaanaaq (Thule) in Greenland and Vostok in Antarctica,
31 respectively. The PC index concept was developed through the pioneering works of Troshichev and
32 Andrezen (1985) and Troshichev et al. (1988). Further PC index developments were made by
33 Vennerstrøm (1991). A fundamental description of the PC index derivation methods and their
34 physical meaning was published by Troshichev et al. (2006).

35 To derive PC index values, magnetic variations related to the transpolar convection of plasma and
36 magnetic fields are calibrated to equal values of the merging electric field (Kan and Lee, 1979) in
37 the undisturbed solar wind. Thus, the PC indices represent the merging processes between the solar
38 wind magnetic fields extending from the Sun and the terrestrial magnetic fields at the front of the
39 magnetosphere and could be considered representative of the energy input from the solar wind. This
40 energy may be temporarily stored in the magnetospheric tail configuration to be dissipated in
41 processes such as auroral substorms, upper atmosphere heating, and ring current enhancements.

42 Final (post-event) PCN and PCS index series have been used to investigate relations between
43 interplanetary parameters and polar cap magnetic disturbances (e.g., Troshichev and Lukianova,
44 2002; Huang, 2005) and the electric potentials in the polar cap ionosphere (e.g., Troshichev et al.,
45 2000; Nagatsuma, 2002; Ridley and Kihn, 2004).

46 The relations between the polar cap indices and auroral activity was studied, among others, by
47 Troshichev and Andrezen (1985), Vennerstrøm et al. (1991), Vassiliadis et al. (1996), Liou et al.
48 (2003), and Huang (2005). The relations between positive and negative PC index values and Joule
49 heating of the atmosphere was investigated by Chun et al. (1999, 2002). Most investigations have
50 given correlation coefficients ranging between 0.6 and 0.8 between polar cap index values and
51 parameters characterizing auroral activity.

52 In substorm studies, Janzhura et al. (2007) have used the PC indices to predict the duration of the
53 growth phase in substorm developments. For isolated events they estimated that substorm onset
54 would occur as the PC index level reached ~ 2 mV/m. From investigations of a large number of
55 substorms, Troshichev et al. (2014) concluded that substorm onset was likely to happen when the
56 PC index starting from a low level exceeded 1.5 ± 0.5 mV/m.

57 In studies of geomagnetic storms by Stauning et al. (2008) and Stauning (2012), the PC indices
58 have been used in source functions to predict the development of ring current intensities
59 characterized by Dst index values. Troshichev and Sormakov (2017) have used PC indices to
60 predict the maximum geomagnetic storm intensities (Dst minima).

61 An important application of real-time PC indices is the forecast of strong substorms that may
62 threaten power grids through their Geomagnetically Induced Current (GIC) effects. An
63 investigation of GIC-related high voltage power line disturbances in Scandinavia (Stauning, 2013c)
64 has demonstrated that the PC index values most often remained at a high level for more than 2-3
65 hours up to the power line cuts. The lengthy pre-event intervals are most likely needed for enabling
66 the merging processes at the front of the magnetosphere and subsequent transpolar convection
67 characterized by the PC index to load the tail configuration with enough energy to generate violent
68 substorm events. The intense merging processes may also be necessary for making the polar cap
69 expand enough to enable substorm activity reaching subauroral latitudes where important power
70 grids reside. According to these investigations, PC index levels above 10 mV/m maintained through
71 more than one hour should cause alert for subauroral power grids.

72 In the past, a diversity of PC index versions have been in play at the above-mentioned (and many
73 further) investigations (Stauning, 2013a), which seriously reduce their scientific value. Thus, much

74 effort has been invested in attempts to generate commonly accepted PC index versions (e.g.,
 75 Troshichev et al., 2006). On basis of the documentation provided in Matzka (2014), new PC index
 76 versions were adopted by IAGA by its Resolution no. 3 (2013) with the text:

77 *IAGA, **noting** that polar cap magnetic activity is not yet described by existing IAGA geomagnetic*
 78 *indices, **considering** that the Polar Cap (PC) index constitutes a quantitative estimate of*
 79 *geomagnetic activity at polar latitudes and serves as a proxy for energy that enters into the*
 80 *magnetosphere during solar wind-magnetosphere coupling, **emphasising** that the usefulness of such*
 81 *an index is dependent on having a continuous data series, **recognising** that the PC index is derived*
 82 *in partnership between the Arctic and Antarctic Research Institute (AARI, Russian Federation) and*
 83 *the National Space Institute, Technical University of Denmark (DTU, Denmark) **recommends** use*
 84 *of the PC index by the international scientific community in its near-real time and definitive forms,*
 85 *and **urges** that all possible efforts be made to maintain continuous operation of all geomagnetic*
 86 *observatories contributing to the PC index.*

87 Thus, the IAGA-recommendations comprise both the final and the near-real time versions of PCN
 88 and PCS indices. Until the final values could be issued, the indices may be available in provisional
 89 versions. At present, the PCN indices are distributed in all versions, while the PCS indices are
 90 distributed in their near-real time and provisional versions only. The indices are distributed from the
 91 web portals <http://pcindex.org> operated by AARI and <http://isgi.unistra.fr> operated by the
 92 International Service for Geomagnetic Indices (ISGI). However, as shall be demonstrated, the near-
 93 real time values as well as the final PC index series are invalidated by inappropriate handling of the
 94 solar wind sector effects introduced by Menvielle et al. (2011) in reference level calculations.

95

96 2. Calculation of Polar Cap indices.

97 The transpolar (noon to midnight) convection of plasma and magnetic fields driven by the
 98 interaction of the solar wind with the magnetosphere generates electric (Hall) currents in the upper
 99 atmosphere. These currents, in turn, induce magnetic variations at ground level (Troshichev et al.,
 100 1988, 2006; Vennerstrøm, 1991). For derivation of PC indices from the recorded magnetic field
 101 series, \mathbf{F} , the horizontal magnetic variations, $\Delta\mathbf{F} = \mathbf{F} - \mathbf{F}_{\text{RL}}$, with respect to an undisturbed reference
 102 level (RL), \mathbf{F}_{RL} , are projected to a direction in space assumed to be perpendicular to the transpolar
 103 convection-related currents in order to focus on solar wind effects. The optimum direction is
 104 characterized by its angle, φ , to the E-W direction. Next, ΔF_{PROJ} values are scaled to make the PC
 105 index equal on the average to the solar wind merging electric field, E_M , (Kan and Lee, 1979). Thus

$$106 \quad \text{PC} = (\Delta F_{\text{PROJ}} - \beta) / \alpha \approx E_M \quad (1)$$

107 The optimum angle, φ , and the propagation delay, τ , between the reference location for the solar
 108 wind data and the location for related effects at the polar cap are both estimated from searching the
 109 optimum correlation between E_M and ΔF_{PROJ} . The calibration constants, the slope, α , and the
 110 intercept, β , are found by linear regression between ΔF_{PROJ} and E_M through an extended epoch of
 111 past data.

112

113 3. PC index reference level.

114 For the reference level from which polar magnetic disturbances are measured, different concepts
 115 have been used. In the version developed by Vennerstrøm (1991), just the secularly varying base
 116 level, \mathbf{F}_{BL} , was used. This level does not reflect the daily magnetic variations during undisturbed
 117 conditions. However, the calibration parameters, notably the intercept coefficient, reflect the
 118 undisturbed daily variation averaged over the epoch used for the regression.

$$119 \quad \mathbf{F}_{RL} = \mathbf{F}_{BL} \quad (\text{Vennerstr\o{m}, 1991}) \quad (2)$$

120 In the version developed at the Arctic and Antarctic Research Institute (AARI) in St. Petersburg,
 121 Russia, the varying level on “*extremely quiescent days*” (Troshichev et al., 2006) was used as the
 122 PC index reference level. This level could be considered built from a quiet day curve (QDC), \mathbf{F}_{QDC} ,
 123 added on top of the base level, \mathbf{F}_{BL} . Thus in vector formulation:

$$124 \quad \mathbf{F}_{RL} = \mathbf{F}_{BL} + \mathbf{F}_{QDC} \quad (\text{AARI, Troshichev et al., 2006}) \quad (3)$$

125 Extremely quiescent days are rare particularly at polar latitudes. Therefore, the concept was
 126 broadened to imply the generation of QDC values from quiet segments of nearby days. The QDC
 127 calculations are detailed in Janzhura and Troshichev (2008) (hereinafter J&T2008). From the
 128 recordings during 30 days at a time, the variability in the 1-min samples within each 20-min section
 129 of recorded data is used to decide whether the section was quiet enough to let the average value be
 130 included in the construction of an initial QDC by superposition of quiet samples. The particular day
 131 for the QDC is determined by the relative amounts of quiet samples and usually positioned at the
 132 middle of the considered interval. The 30 days interval is then shifted forward and the QDC
 133 calculations repeated to be referred to another (or eventually the same) day. Finally, from the
 134 sequence of initial 30-days QDCs the final QDCs for any of the days are found by smoothing
 135 interpolation. It should be noted that the choice of using 30 days interval at a time implies evening
 136 out possible solar wind sector (SWS)-related effects which may have cyclic variations with the 27.4
 137 days solar rotation. (the notation “SWS” is used here instead of “SS” used elsewhere).

138 In order to handle the SWS-related variations, \mathbf{F}_{SWS} , caused mainly by the effects from the Y-
 139 component, IMF B_Y , of the Interplanetary Magnetic field (IMF), on the convection patterns, it was
 140 suggested by Menvielle et al. (2011) that the reference level should be constructed from using a
 141 particular solar wind sector term, \mathbf{F}_{SWS} , added to the base level and the regular QDC.

$$142 \quad \mathbf{F}_{RL} = \mathbf{F}_{BL} + \mathbf{F}_{QDC} + \mathbf{F}_{SWS} \quad (\text{Menvielle et al., 2011}) \quad (4)$$

143 It should be noted that this concept marks an infringement of the QDC definition in Troshichev et
 144 al. (2006) by introducing a reference level contribution, \mathbf{F}_{SWS} , which is not necessarily quiet. There
 145 is no validation of this concept or reference to its origin in Menvielle et al. (2011).

146 The SWS concept is further specified in Janzhura and Troshichev (2011) (hereinafter J&T2011). At
 147 the interaction between the solar wind and the magnetosphere, as explained in J&T2011, the IMF
 148 By components generate field-aligned currents (FAC) and associated horizontal currents in the
 149 Cusp region near local noon at 75-80° geomagnetic latitude. In p. 1492 of J&T2011 they state that
 150 “*the QDC level displays long-term changes, which are determined by the sector structure*”. Further
 151 they state “*Thus, if we are going to analyze the polar cap magnetic activity produced by the IMF*
 152 *fluctuations related to disturbed solar wind, we have to exclude first the sector structure effect*”.

153 One implication of their statement is that the IMF B_Y component when varying slowly (few days to
 154 2 weeks) is not affecting the polar magnetic disturbance levels. The issue has not been properly
 155 validated and the implication might be incorrect. The second issue, which shall be discussed to
 156 some extent here, is whether the applied data handling techniques actually remove the sector
 157 structure effects or just (as will be shown) generate inconsistent features and odd results.

158 In J&T2011 the sector structure effects are derived from daily median values of the recorded polar
 159 magnetic fields that vary with the IMF B_Y component in the solar wind. In the post-event version,
 160 the SWS terms are derived from daily median values smoothed over 7 days with the day of interest
 161 at the middle. In the near-real time version the actual day’s SWS value is derived by cubic spline-
 162 based extrapolation of past daily median values. The regular 30-days QDC is derived from the
 163 recorded data less the SWS effect. Thus:

$$164 \quad \mathbf{F}_{RL} = \mathbf{F}_{BL} + \mathbf{F}_{SWS} + \mathbf{F}_{QDC,SWS} \quad (\text{Janzhura and Troshichev, 2011}) \quad (5)$$

165 For the IAGA-endorsed version (Matzka, 2014), the base level in the AARI version in Eq. 3
 166 (Troshichev et al., 2006) is replaced by a median-based level, \mathbf{F}_M . The modified QDC term,
 167 $\mathbf{F}_{QDC,SWS}$, is derived from the data series, \mathbf{F} , less the \mathbf{F}_M values.

$$168 \quad \mathbf{F}_{RL} = \mathbf{F}_M + \mathbf{F}_{QDC,SWS} = \mathbf{F}_{BL} + \mathbf{F}_{SWS} + \mathbf{F}_{QDC,SWS} \quad (\text{IAGA, Matzka, 2014}) \quad (6)$$

169 Actually, this is the same concept as the one defined in J&T2011 except that the secular variations
 170 are now included in the median values (Nielsen and Willer, 2019) instead of being included in the
 171 base line values. Thus, the IAGA concept could be discussed on basis of the J&T2011 publication,
 172 which – so far – holds the only existing presentation of the QDC and SWS properties from the
 173 providers of the IAGA endorsed PC indices. The SWS concept has been discussed in Stauning
 174 (2013b, 2015, and 2018a,c).

175

176 **4. Reference levels for PC index calculations in the IAGA-endorsed post-event (final) version.**

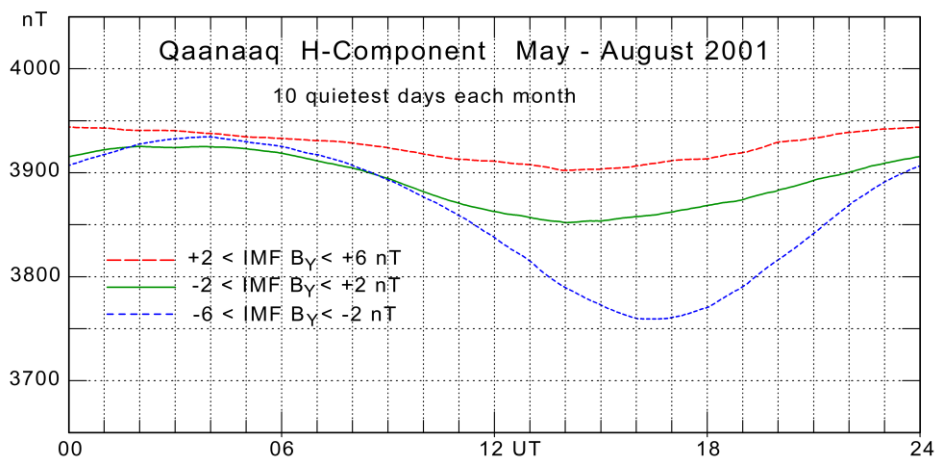
177 The IMF B_Y -related variations in the daily course of the polar magnetic field components are
 178 important for calculations of the reference level for PC index calculations. It should be noted that
 179 the local time 24 h cycle represents the daily course in the observatory position relative to the Cusp
 180 region located close to local noon at magnetic latitudes a few degrees equatorward of Qaanaaq
 181 latitude.

182 Like noted at p. 1492 in J&T2011, “*the azimuthal IMF component controls the BY FAC (field-*
 183 *aligned current) system observed in the day-time cusp region during the summer season*”. Thus, the
 184 anticipated IMF B_Y -related effects on the convection patterns should maximize near noon and be
 185 reduced near midnight when the observatory location is farthest away from the Cusp. For Qaanaaq
 186 data this tendency is seen most clearly in displays of the H- (or Y-) component variations.

187 The interval from days 145 to 245 of 2001 is discussed in J&T2011 and therefore selected for a
 188 closer examination of data and derived values here. Fig. 5b of J&T2011 displays the average daily
 189 variations in the H-components (all samples) recorded at Qaanaaq during the summer months, May-
 190 August, of 2001 for different levels of IMF B_Y . For the same data interval, Fig. 1 here displays the
 191 corresponding IMF B_Y -related daily variations for the quietest days only. Values of the IMF B_Y
 192 component are derived from OMNIweb interplanetary satellite data service
 193 (<http://omniweb.gsfc.nasa.gov>).

194 The results in Fig. 1 are largely the same as those of Fig. 5b in J&T2011. Local midnight at
 195 Qaanaaq is at around 04 UT, noon at 16 UT. It is seen in both diagrams that the variations with IMF
 196 B_Y are small during the night while the daytime values, and thus the amplitude in the daily
 197 variation, depend strongly on the IMF B_Y level.

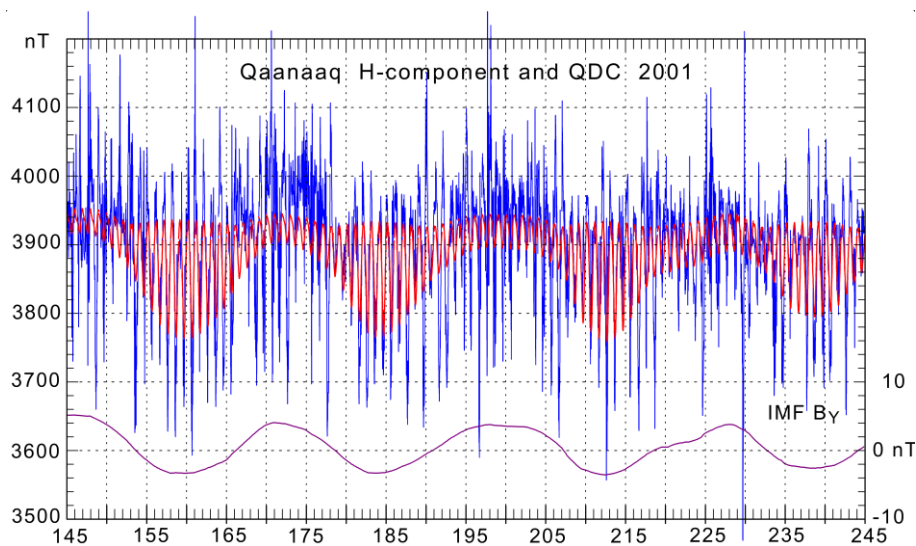
198



199

200 **Figure 1.** Mean daily variation in the H-component at Qaanaaq (Thule) during the 10 quietest days of each
 201 of the summer months of 2001 derived for three gradations of the IMF azimuthal component: $+2 < B_Y < +6$
 202 nT (upper red line), $-2 < B_Y < +2$ nT (green line), and $-6 < B_Y < -2$ nT (lower blue line).
 203

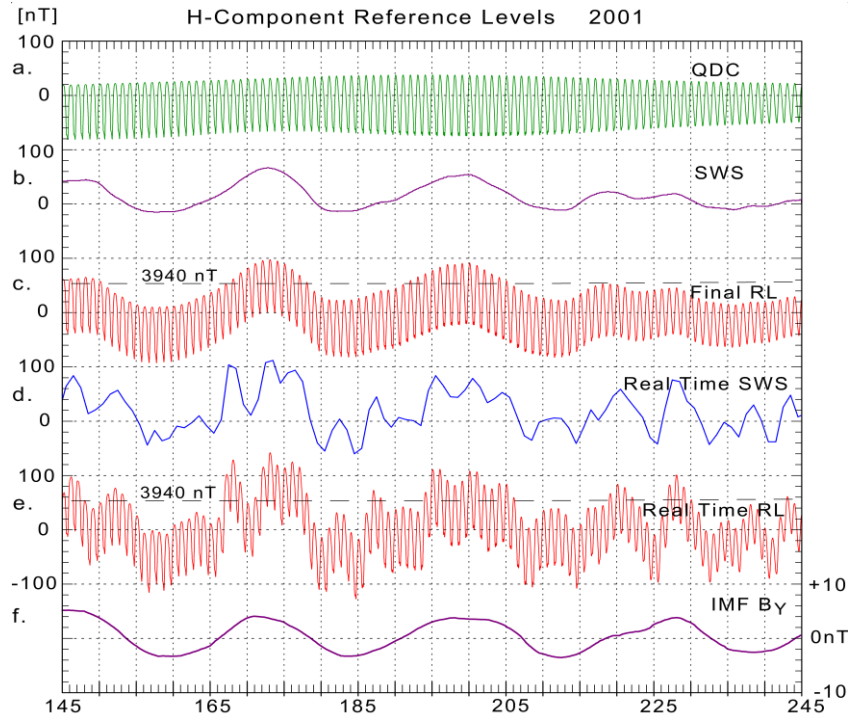
204 With the variations of the QDC values with IMF B_Y displayed in Fig. 1 during the months centred
 205 on 1 July and corresponding displays centred at different dates, the QDC values throughout the
 206 selected interval could be constructed. The resulting QDCs taking the seasonal as well as the IMF
 207 B_Y -related variations into account are displayed by the curve in heavy red line superimposed on the
 208 observed values of the H-component shown in Fig. 2. Smoothed values of IMF B_Y are displayed by the
 209 lower curve with reference to the right scale. The upper envelope of the QDC values presents the
 210 night H-component values and varies little with IMF B_Y while the lower envelope, which presents
 211 the midday QDC values, varies strongly with IMF B_Y in agreement with the display in Fig. 1. These
 212 QDCs could be considered to represent idealized QDC levels for the summer season of year 2001.



213

214 **Figure 2.** QDCs (red line) based on quiet data only superimposed on recorded H-component values (blue
 215 line). Smoothed values of IMF B_Y (magenta line) on right scale are shown at the bottom.
 216

217 For the IAGA-endorsed post-event (final) PC index version, Fig. 3 displays the construction of the
 218 reference levels. The upper three fields are based on interim values derived from PCN index
 219 calculations and supplied from the PCN index provider at DTU Space. For reference, the bottom
 220 curve (f) displays smoothed values of the IMF B_Y component (same as those displayed in Fig. 2).
 221



222
223

224
225
226
227
228

Figure 3. IAGA-endorsed constructions of H-component reference levels for PCN throughout days 145 to 245 of 2001 for final and real-time PCN index versions. (a.) Final QDC_{SWS} . (b.) Final SWS terms. (c.) Final reference levels, RL. (d.) Real-time SWS terms. (e.) Real-time reference levels. (f.) Smoothed IMF B_Y (on right scale).

229
230
231
232
233
234

The upper curve (a) in Fig. 3 displays the 30-days QDC_{SWS} values for the Qaanaaq H-component derived according to the method defined in J&T2008 but based on recorded quiet data less the SWS terms. The next lower curve (b) displays the SWS terms derived as the differences (cf. Eq. 6) between the 7-days smoothed daily median values and the secularly varying base line values interpolated between the yearly defined values (also supplied from DTU Space). The 0 nT dotted line represents base line values varying between 3895 nT on day 145 and 3899 nT on day 245.

235
236
237
238
239
240
241

The next lower curve (c) displays the resulting H-component reference level formed as the sum of the H_{SWS} and $H_{QDC,SWS}$ values. The horizontal dashed line across this curve (c) presents the uppermost level (3940 nT) of the mean H-component values in Fig. 1 (or Fig. 5 of J&T2011). Curve (c) is an almost exact replica of the H-component reference curve displayed in heavy line in Fig. 1 of J&T2011 for which the caption states “*the quiet daily curve (QDC) characterizing the daily variation of the quiet geomagnetic field*”. However, there are serious problems with this choice of reference level:

242
243
244
245

(i) Contrary to the caption for Fig. 1 of J&T2011, the reference level is not “quiet” being composed from the sum of a quiet part and a median-based part that varies with the disturbance level.

(ii) The daily variations in the components imposed by the reference level construction are not in agreement with observed daily variations during corresponding conditions.

246
247
248
249
250

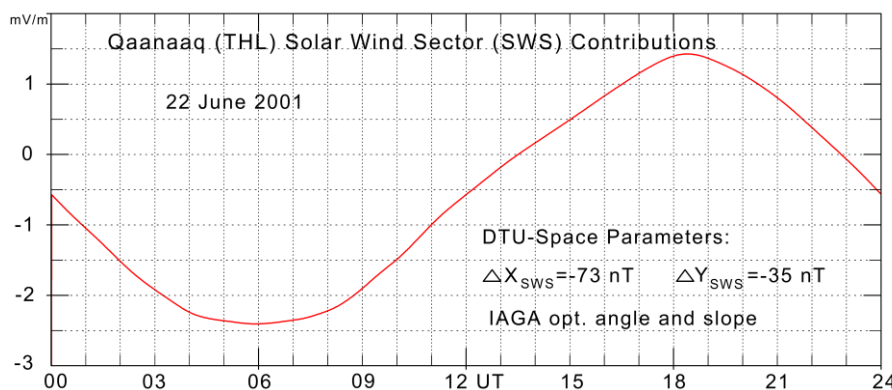
(iii) The upper envelope which represents night values of the daily variations in the H-component varies strongly with the varying IMF B_Y level contrary to night values in Fig. 1 (or Fig. 5 of J&T2011). Some of the night reference values exceed considerably the uppermost statistical average values for corresponding IMF B_Y conditions whether based on all data (Fig. 5 of J&T2011) or just quiet values (Fig. 1 here).

251 (iv) The amplitudes in the daily variation display seasonal variations only and do not vary with the
 252 IMF B_Y level contrary to the strong amplitude variations seen in Fig. 1 (or Fig. 5 of J&T2011). For
 253 June (days 152-181) of 2001 the amplitudes in the reference level variations remain at appr. 100 nT,
 254 while in Fig. 1 the amplitudes vary with the relevant IMF B_Y levels (-3 to +4 nT) between appr. 50
 255 and 150 nT.

256 (v) Using the reference levels from Fig. 3 and the corresponding levels for the D-component at
 257 index calculations generates peculiar daily variations in the SWS-related contributions to the PCN
 258 index.

259 The SWS term, F_{SWS} , is a vector rotating with the Earth and must be projected to the optimum
 260 direction in space to derive its contribution to the PC index. During 24 hours the projected term
 261 varies between + and - the maximum amplitude reached at two locations, one at daytime the other
 262 at night, when the F_{SWS} direction is parallel (or antiparallel) to the optimum direction. According to
 263 Eq. 1, the effect on the PC index is $\Delta PC_{SWS} = F_{SWS,PROJ} / \alpha$. The slope values, α , are around two
 264 times larger at day than at night (cf. tables at <http://pcindex.org>). Thus, with the present calculation
 265 scheme, the nighttime ΔPC_{SWS} , inevitably, will be around twice the daytime contributions although
 266 the IMF B_Y -related SWS effects caused by current systems at the Cusp region near noon in local
 267 time (Wilhjelm et al., 1972; Iijima and Potemra, 1976) should maximize there. This obvious
 268 conflict was addressed in Stauning (2013b and 2015).

269 Using both the H- and the D-components (or the X- and Y-components) of the data supplied from
 270 DTU Space enables specific calculations of the SWS effects on the PCN indices. The calibration
 271 parameters (φ, α, β) published at <http://pcindex.org> by the index providers have been used in the
 272 calculation of the contributions. The result for a selected day, 22 June 2001, is shown in Fig. 4.



273
 274 **Figure 4.** Variations in the SWS-related contributions to the PCN index on 22 June 2001 based on data and
 275 base line values supplied from DTU Space. (similar to Fig. 4 of Stauning, 2015)
 276

277 The display in Fig. 4 based on the data supplied from DTU Space is very close to the results
 278 presented in Fig. 4 of Stauning (2015) based on the data presented in J&T2011. The most
 279 controversial feature is the (numerical) maximum in the IMF B_Y -related SWS contributions to the
 280 PCN index values at night with a depression of 2.5 mV/m at 06:30 UT near local midnight (04 UT).
 281 At this time, the THL observatory is farthest away from the Cusp region where the IMF B_Y -related
 282 effects originate. The contribution is small at local noon (16 UT) where the observatory is closest to
 283 the Cusp region. The largest positive contribution of 1.5 mV/m is seen at 18:30 UT, a few hours
 284 past local noon.

285 A basic error in the method is the implied assumption that a SWS term calculated from daily
 286 median values can be applied throughout the whole day to remove SWS effects disregarding the
 287 variations of the IMF B_Y -related solar wind sector effects with the varying observatory position in

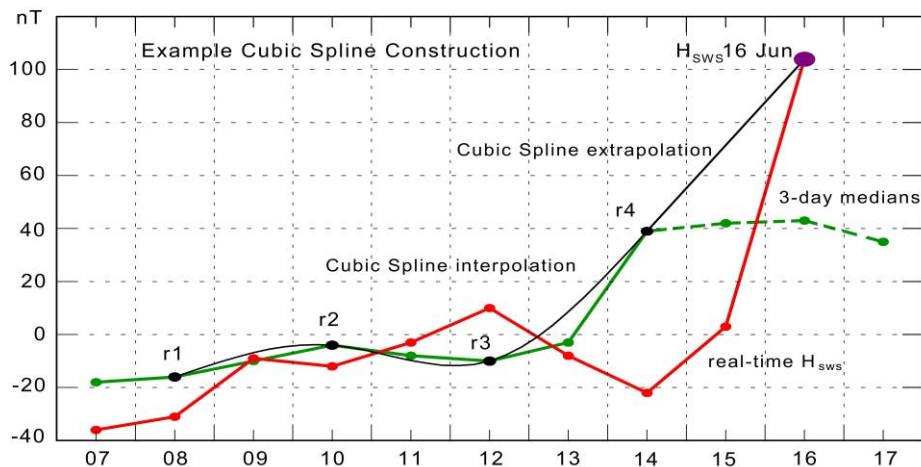
288 the polar cap. The real SWS effects could even be opposite of the effects calculated from the
 289 constructed SWS values derived by the median-based method.

290 The example calculations displayed in Fig. 4 were based on the case presented in J&T2011 with a
 291 smoothed IMF B_Y value of 4 nT, which is not uncommon. Unjustified SWS contributions of 3-4
 292 mV/m could be expected for the stronger cases (larger IMF B_Y). Such magnitudes are around twice
 293 the onset level of around 2 mV/m for magnetic storm or substorm activity (Troshichev et al., 2014).

294

295 5. Reference levels for PC index calculations in the IAGA-endorsed near-real time version.

296 For real-time calculations of PC index values, which is an important issue for Space Weather
 297 monitoring and forecasting, the 7-day smoothing of median values used for the final version is no
 298 longer applicable. Instead, a cubic spline extrapolation method specified in J&T2011 is applied to
 299 derive the actual SWS terms from past median values. The method uses 3-days average median
 300 values calculated every other of the past 9 days to derive cubic spline polynomials, which are
 301 subsequently extended forward to define the actual SWS value. Based on data from the examined
 302 interval of June 2001, the method is illustrated in Fig. 5 using the terminology from J&T2011.



303

304 **Figure 5.** Details of the cubic spline construction (in black line) of the real-time solar sector term, H_{SWS} ,
 305 from 3-day medians (in green line). The selected four 3-day median values used for the construction of H_{SWS}
 306 on 16 June 2001 are marked by black dots superimposed on the green ones. The cubic spline interpolation
 307 curve and its extrapolation to define real-time H_{SWS} on 16 June are displayed in black line. The dots
 308 connected by the red line represent H_{SWS} values derived by the same method on earlier dates in June 2001.
 309

310 Fig. 5 demonstrates the cubic spline construction for deriving the SWS term on 16 June, 2001. The
 311 3-day median values (green dots) named according to the J&T2011 procedure by r1 (13-15), r2 (11-
 312 13), r3 (9-11), and r4 (7-9 June) are marked by black dots superimposed on the green ones. The
 313 natural cubic spline polynomials have been derived from these 4 points and define the curve in
 314 black line connecting the points. With the slope defined at the last point (14 June) the cubic spline
 315 construction is extended tangentially to 16 June where the resulting H_{SWS} value (103 nT) is marked
 316 by a large black dot.

317 The dots (red) connected by a red line display the H_{SWS} values derived the same way for further
 318 days within the interval from 7 to 16 June using past data only. The 3-day median values on 15, 16
 319 and 17 June connected by the green dashed line segments were not available at the real-time
 320 construction of H_{SWS} for 16 June. They have been added to the figure for illustration of the “take-
 321 off” effects of the cubic spline extrapolation construction that generates the large deviation of the
 322 extrapolated SWS values compared to the post-event smoothed values (cf. Figs. 3 and 6). This is an

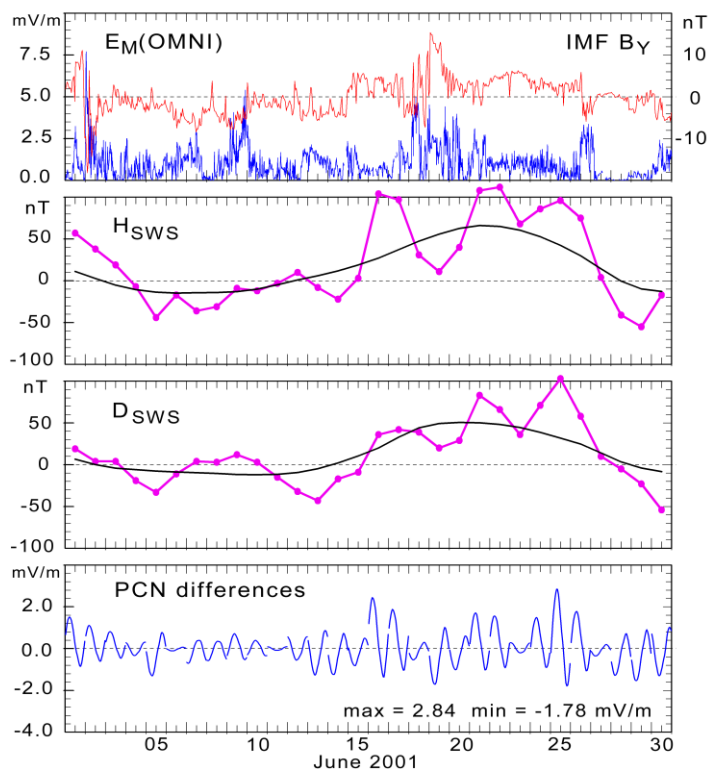
323 inherent effect when using the devised “near-real time” method from J&T2011 to calculate solar
 324 sector effects. A similar figure for a different interval may be seen in Stauning, 2018c.

325 The real time H_{SWS} values for 7-16 June 2001 displayed in Fig. 5 along with the corresponding
 326 H_{SWS} values calculated the same way for the remainder of the days 145-245 of 2001 have been
 327 inserted as the jagged curve (d) in Fig. 3. It should be noted that these values differ from the values
 328 presented by the smooth H_{SS} curve in Fig. 6 of J&T2011, which, contrary to their statements in p.
 329 1496, have not been generated by the devised real-time method but derived from smoothed median
 330 values like the nearly identical values (from DTU Space) displayed by curve (b) in Fig 3.

331 According to the principles for near-real time PC index calculations defined in J&T2008, the 30-
 332 days QDC should be derived by adjusting the most recent 30-days QDC using the seasonal trend
 333 from last year’s QDCs. Since the QDCs in the formulation of J&T2011 (or Matzka, 2014) are
 334 derived from observed data less the SWS terms there is an obvious flaw in the arguments since the
 335 SWS-conditions are not necessarily the same at corresponding dates in different years.

336 Taking a short-cut by assuming that the actual near-real time $H_{QDC,SWS}$ values are the same as the
 337 final $H_{QDC,SWS}$ values displayed by curve (a) of Fig. 3 results in the near-real time H-component
 338 reference level displayed by curve (e) in Fig. 3. The corresponding process would provide the D-
 339 component near-real time values. It is clear from comparing the reference levels defined for the
 340 final version (curve c of Fig. 3) with those of the near-real time version (curve e) that PCN values
 341 calculated by the near-real time method must differ considerably from index values derived by the
 342 post-event method. The resulting effects on the differences between real-time and post-event (final)
 343 PCN values throughout June 2001 are displayed in the bottom panel of Fig. 6.

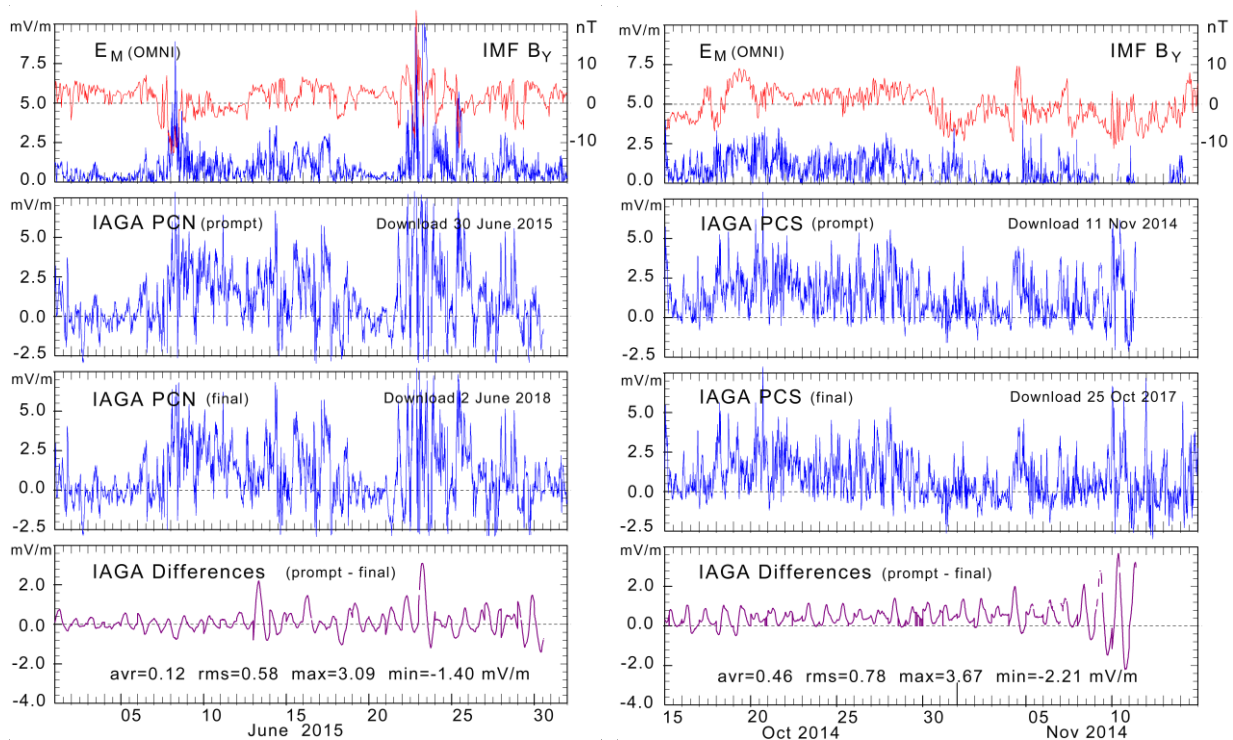
344



345

346 **Figure 6.** From top: Solar wind merging electric field (blue line, left scale) and IMF B_Y component (red line,
 347 right scale), H_{SWS} (real-time) in magenta line and H_{SWS} (final) in black line, D_{SWS} (real time) and D_{SWS} (final),
 348 and (in bottom panel) differences between real-time and final PCN values. Peak differences are noted.
 349

350 The differences of up to 2.84 mV/m have been calculated from the final (smoothed) and the near-
 351 real time cubic spline extrapolated SWS vectors using consolidated calibration parameters
 352 (<http://pcindex.org>). The calculated examples agree well with results obtained from occasional
 353 downloads of near-real time PCN and PCS values compared to the same index series downloaded at
 354 much later times. Differences of up to 3.09 mV/m for PCN (Stauning, 2018c) and up to 3.67 mV/m
 355 for PCS (Stauning, 2018a) were found in the examples displayed in Fig. 7. Such differences related
 356 to using cubic spline extrapolated instead of smoothed values of SWS terms may come on top of the
 357 unjustified SWS contributions discussed in section 4. The example in Fig. 7, furthermore, indicates
 358 that the SWS effects, which generate large index differences by their different handling in the near-
 359 real time and post-event versions, are equally strong at the Southern Polar Cap. This result is
 360 contrary to the statement of the opposite in pp. 1492-1493 of J&T2011 where SWS-effects are
 361 considered negligible for PCS values derived on basis of magnetic data from Vostok on the
 362 Antarctic ice cap.



363
 364 **Figure 7.** Differences between IAGA-endorsed versions of recorded 15-min values of near-real
 365 time and final PCN (left) and PCS (right) indices. (from Stauning, 2018a,c)
 366

367 In Fig. 7 the real-time values are those seen at the end of the traces termed “prompt”. The remaining
 368 parts of the prompt traces are “post-event” values where the approximation to the “final” values is
 369 thought to be gradually improved as more post-event data become available from dates up to the
 370 download time. However, the largest excursions, 3.09 mV/m in PCN and -3.67 mV/m in PCS, are
 371 seen at dates prior to the real-time days. Details of the IAGA-endorsed calculation methods are not
 372 available for further examination of this issue.

373 374 6. Reference levels for PC index calculations in the DMI version.

375 In the DMI PC index version (Stauning, 2016), the definition of the “solar rotation weighted”
 376 (SRW) reference level construction published in Stauning (2011) returns to the statements in
 377 Troshichev et al. (2006) with the vector formulation in Eq. 3, and to the methods outlined in

378 J&T2008. The essential point for the SRW method is deriving the reference level from quiet
 379 samples collected at conditions otherwise as close as possible to those prevailing at the day of
 380 interest. The factors of primary importance are:

- 381 (i) Sample “quietness”
- 382 (ii) Separation of samples from QDC date
- 383 (iii) Solar wind conditions (particularly IMF B_Y and V_{SW})
- 384 (iv) Solar UV and X-ray illumination (based on solar radio flux F10.7 values)

385 For these factors weight functions are defined. For each hour of the day, observed hourly average
 386 values at corresponding hours within an extended interval (± 40 days) are multiplied by the relevant
 387 weights, added and then divided by the sum of weights to provide the hourly QDC value.
 388 Subsequently, the hourly QDC values are smoothed to remove irregular fluctuations and
 389 interpolated to provide any more detailed resolution as required.

390 The weight function for sample quietness is determined from the variability of 1-min data values
 391 within the hour much like the technique used by J&T2008. Two parameters are calculated on a
 392 vector basis. One is the maximum time derivative used to indicate the smoothness within the sample
 393 hour. The other is the average variance to define the slope of data values. Both parameters need to
 394 take small values for the hourly sample to be considered “quiet” (flat and featureless display).

395 For an estimate of further weight functions, the factors of importance were subjected to an
 396 autocorrelation analysis vs. separation between the date of interest and the dates of the samples to
 397 be included in the construction of the QDC values.

398 Details of the autocorrelation are provided in Stauning (2011). The main results were, as expected,
 399 high autocorrelation values at nearby dates and also high values at dates displaced one full solar
 400 rotation of 27.4 days from the day of interest where the solar illumination and the solar wind
 401 conditions were similar on a statistical basis to the prevailing conditions. In between, at half a solar
 402 rotation, mixed autocorrelation results were found. In some cases a local maximum was seen
 403 indicating the occurrence of 4-sector solar wind structures. In most cases the autocorrelation
 404 function had a deep minimum at half a solar rotation indicating 2-sector structures. For the solar
 405 rotation weighting a squared cosine function was selected to provide unity weights at the QDC date
 406 (zero separation), and at dates separated by 27.4 days, and zero weight at half a solar rotation period
 407 when the opposite face of the Sun is pointing toward the Earth and the solar wind sector effect,
 408 most likely, is in the opposite direction (2-sector structure) or weak (multi-sector structure) (cf. Fig.
 409 6 of Stauning, 2013a).

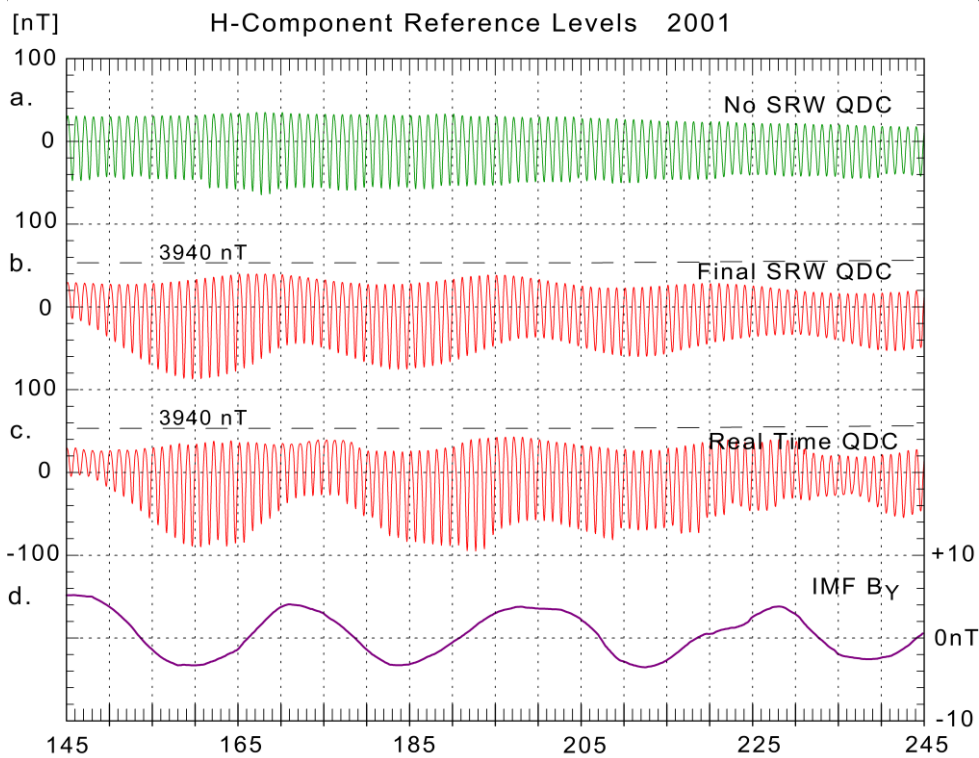
410 The final weight factors for sample separation have a central maximum holding 50% of the total
 411 weights and two secondary maxima at a solar rotation period (27.4 days) before and after the QDC
 412 day holding weights corresponding to 25% of the total weight each. The total span of samples
 413 included in the QDC construction is set to ± 40 days to encompass all three weight maxima. The
 414 separation weight factors are pre-calculated (see Stauning, 2011).

415 As data are collected the quietness weight factors can be calculated promptly for each hour of
 416 recordings along with the hourly averages of each component. The three values are stored. The
 417 quietness weight factors are common for the two horizontal components and independent on their
 418 representation in (X,Y) or (H,D) coordinates.

419 Thus, at any time after 80 days of data collection, the relevant final QDC could be calculated for
 420 any day more than 40 days in the past. The hourly component averages and their quietness weight
 421 factors are fetched from their stored values and their separation weight factors are found from the
 422 tabulated values. For each hour of the day, the hourly average component values within ± 40 days

423 are multiplied by the weight factors and summarized. The products of weight factors are
 424 summarized. The sum of weighted component hourly average values is divided by the sum of
 425 weights to define the hourly QDC value.

426 The weighting technique allows calculations of real-time QDCs with reduced accuracy by simply
 427 ignoring missing samples without changing the calculation scheme. The DMI SRW-method is
 428 illustrated in Fig. 7 in a format similar to Fig. 3 with smoothed values of IMF B_y displayed by the
 429 bottom curve (d). The uppermost curve (a) display H_{QDC} values derived by weighting the samples
 430 collected at corresponding hours over ± 40 days with their “quietness” factors only disregarding the
 431 solar rotation weight factors. Curve (b) displays post-event (final) solar rotation-weighted H-QDC
 432 values. The next lower curve (c) displays real-time H-QDC values derived by using the SRW
 433 calculation scheme but including pre-event samples only (Half solar rotation weighting, HSRW).
 434



435
436

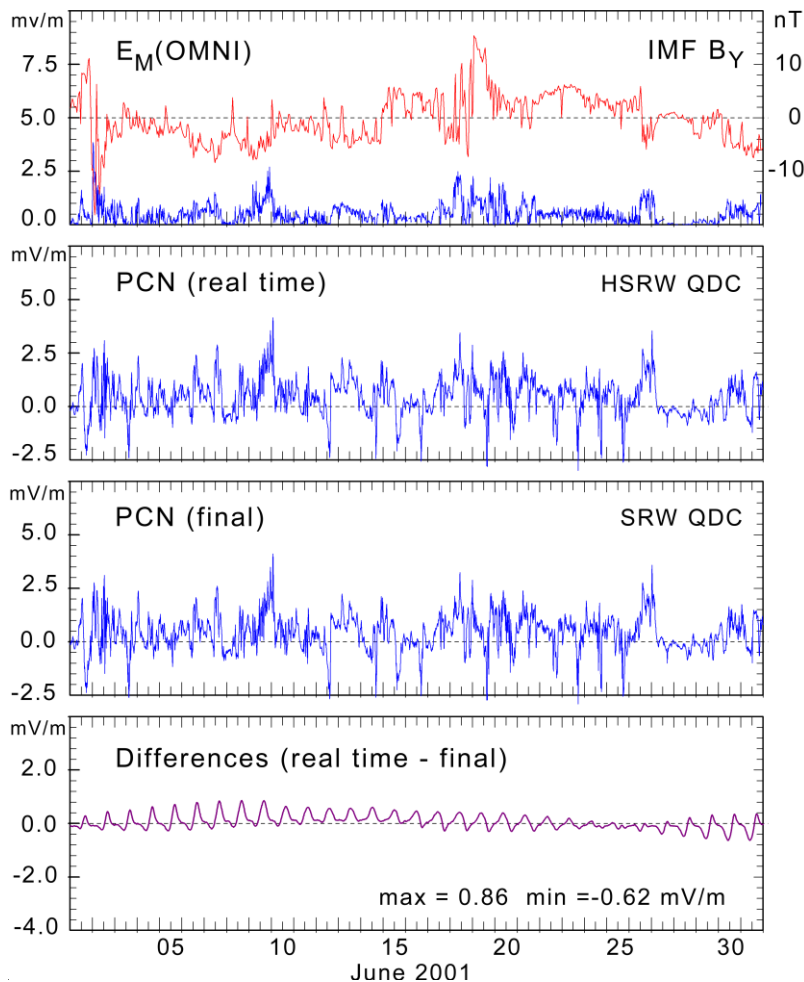
437 **Figure 8.** DMI solar rotation weighted (SRW) QDC reference values. (a) QDC with quietness weighting
 438 only. (b) Post-event (final) SRW QDC. (c) Real-time (HSRW) QDC values built from past samples only. (d)
 439 Smoothed IMF B_y values.
 440

441 The upper envelope (night values) of the SRW QDC reference values in curve (b) displays small
 442 variations with IMF B_y while the lower envelope (midday values) and the amplitudes in the daily
 443 variation displays much stronger variations with IMF B_y as anticipated from the features seen in
 444 Figs. 1 and 2 here (and Fig. 5 of J&T2011). The final QDCs in curve (b) should be compared to the
 445 reference levels in curve (c) in Fig. 3. The real-time QDCs in curve (c) in Fig. 8 based on using past
 446 data only (0 to -40 days) display more irregular variations than the QDCs based on the full amount
 447 (± 40 days) as could be expected. However, the real-time reference QDCs in curve (c) in Fig. 8
 448 should be contrasted to the jagged reference levels displayed by curve (e) in Fig. 3. The horizontal
 449 dashed lines across the two middle fields present the uppermost level of average H-component
 450 values in Fig. 1 (like those drawn in Fig. 3). It is seen that the QDC reference values here – contrary

451 to the reference levels displayed in Fig. 3 – remain below the uppermost level of statistical mean
 452 values for the relevant IMF B_Y ranges.

453 An example of the relations between post-event (final) and real-time PCN index values is depicted
 454 in Fig. 9 using data from the previously selected interval spanning days 145-245 of year 2001.

455



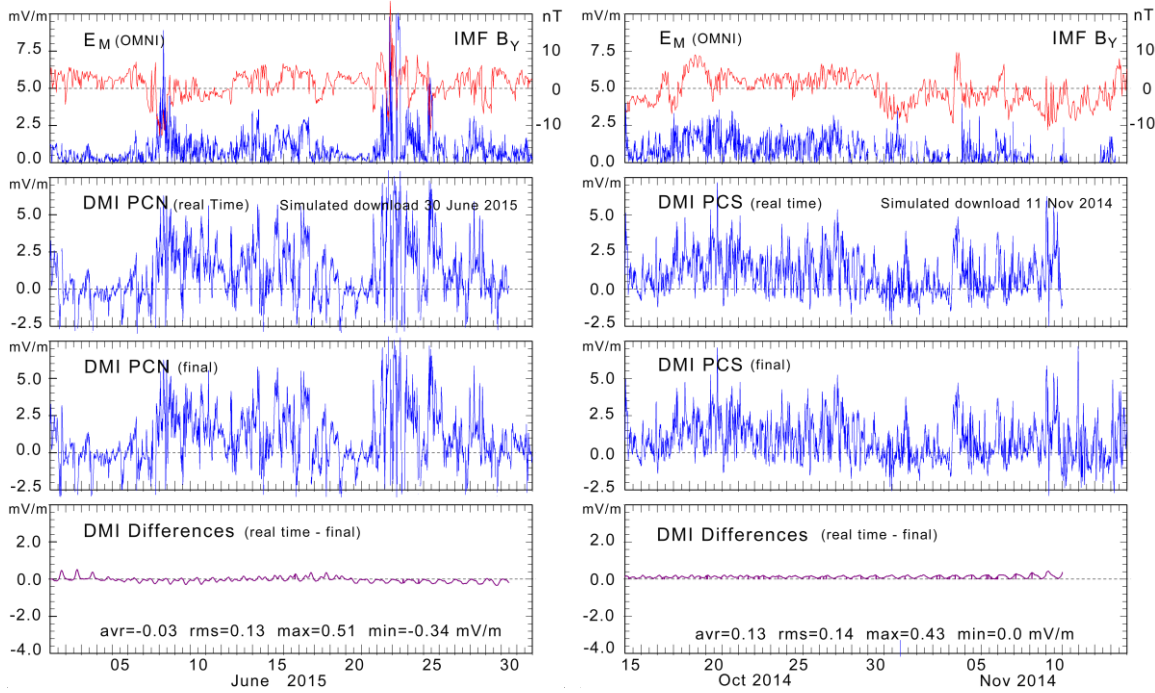
456

457 **Figure 9.** Example of differences between real-time and final PCN values derived by using HSRW QDCs
 458 on past data from days -40 to present day only and SRW QDC using the full ± 40 days sampling interval.

459

460 The differences displayed in the bottom field of Fig. 9 should be contrasted to those displayed at the
 461 bottom field of Fig. 6 on the same scale. It is seen that the differences between calculated real-time
 462 and post-event PCN index values have been reduced considerably.

463 In Fig. 7 the prompt index values were downloaded from the web portal <http://pcindex.org> in near-
 464 real time, while the post-event (final) index values were downloaded at a much later time. For
 465 further comparisons of IAGA-endorsed methods with the present DMI calculation scheme, Fig. 10
 466 presents for the same dates real-time values of PCN and PCS, which have been constructed from
 467 past data using HSRW QDC values on pre-event data only, while the post-event (final) PCN and
 468 PCS values have been derived by using the full ± 40 days SRW-QDCs.

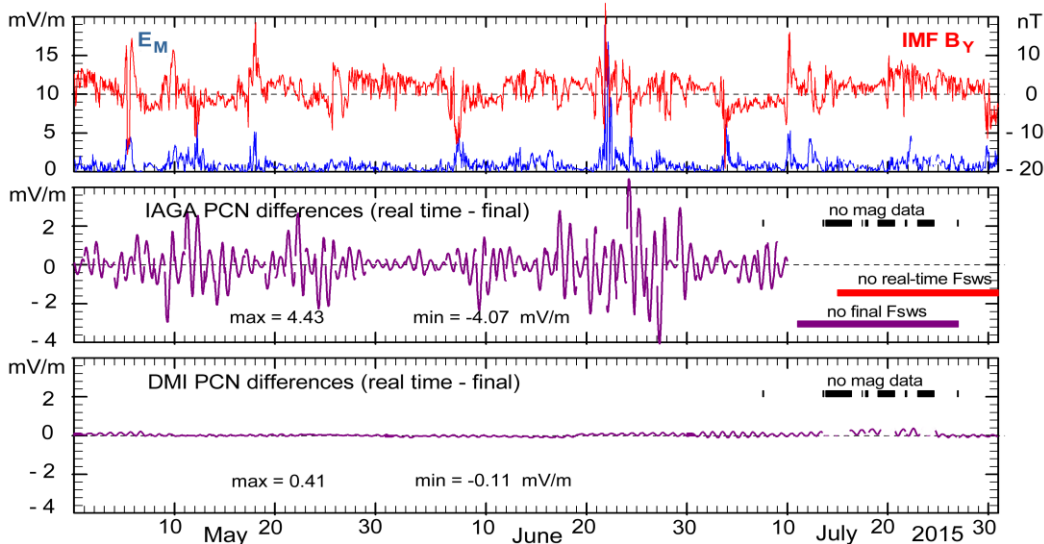


469

470 **Figure 10.** PCN and PCS real-time 15-min values calculated for simulated downloads by using pre-event
 471 data only in HSRW QDCs. PCN and PCS final values were calculated by using full SRW QDCs.
 472

473 Comparing the differences between prompt and post-event PC index values in Fig. 10 with those
 474 displayed in Fig. 7 demonstrates the strongly reduced differences obtained by using the HSRW
 475 QDC derivation scheme instead of the IAGA-endorsed cubic spline extrapolation method.

476 An example of both the reduced differences between real-time and final PC index values and the
 477 increased robustness to missing data with the DMI method compared to the IAGA-endorsed method
 478 is shown in Fig. 11 from Stauning (2018c). The calculations are based on Qaanaaq (THL) data from
 479 2015, which were exposed to irregular recordings at the end of July.



480

481 **Figure 11.** Differences between PCN hourly index values calculated by using real-time and final values of
 482 F_{SWS} in the IAGA-endorsed versions in the middle field and the corresponding differences for the PCN
 483 indices in the DMI versions in the bottom field. Intervals of missing values are marked in both lower fields.
 484 (from Stauning, 2018c).

485 PCN index values could not (of course) be calculated where data are missing. The reference levels
486 in the IAGA-endorsed versions are strongly affected by the missing or corrupted median values
487 throughout intervals extending beyond the sections of missing data. The “IAGA PCN differences”
488 of up to more than 4 mV/m in Fig. 11 have been calculated from solar sector terms derived by using
489 the procedure defined in J&T2011.

490 For Space Weather applications the risk of false PC index values caused by missing data throughout
491 parts of the days, which may cause large displacements of their median values, is probably still
492 more important than missing index data. In an example discussed in Stauning (2018c), where data
493 were made unavailable for 12 hours, the post-event PC index values were changed significantly
494 throughout 13 days centred at the disturbed day. The near-real time indices were changed
495 throughout 8 days after the disturbance by up to 4 mV/m occurring 2 days after the interval of
496 unavailable data. Such amounts may falsely indicate (or hide) strong magnetic storm conditions
497 without warnings.

498 In Fig. 11, the “DMI PCN differences” between real-time and final PCN index values in the
499 versions based on the SRW techniques remain small (below 0.5 mV/m) and almost unaffected by
500 intervals of missing data. In addition, and of prime importance for the potential use of real-time PC
501 indices in Space Weather monitoring, the SRW-based QDC method, as evident from Fig. 11, is far
502 more robust to data supply irregularities than the cubic spline-based forward extrapolation
503 technique that depends critically on the completeness of data samples.

504 The application of the DMI methods defined in Stauning (2016), to derive real-time and final PC
505 index values from polar magnetic data assumed currently available, is detailed in the appendix to
506 Stauning (2018c). Relevant magnetic data might be obtained for qualified PCN and PCS
507 calculations from further observatories in the central polar regions like Resolute Bay and Dome-C
508 beyond the standard observatories, Qaanaaq and Vostok.

509

510

511 **7. Discussions**

512 It should be stressed that the median-based reference levels used in the IAGA-endorsed versions are
513 not quiet levels and thus differ from previous real or verbal definitions of the PC index reference
514 level in publications included those listed as supporting references in the IAGA endorsement
515 documentation written by Matzka (2014) (e.g., Troshichev et al., 2006; Janzhura and Troshichev,
516 2008; Troshichev, 2011; Janzhura and Troshichev, 2011, Troshichev and Janzhura, 2012a;
517 Troshichev and Janzhura, 2012b). Even at the web portal (<http://isgi.unistra.fr>) of the International
518 Service of Geomagnetic Indices, ISGI, the PC index definition states (incorrectly) that index values
519 are derived from deviations from the quiet level. The use of median-based reference levels has
520 never been validated in publications and must be considered based on an unjustified postulate
521 originating in Menvielle et al. (2011) and further specified in Janzhura and Troshichev (2011).

522 A main objection against the IAGA-endorsed reference level construction is the resulting local time
523 variation in IMF B_Y -related effects seen in the H-QDC component in Fig 3 or in the effects on the
524 PCN index values seen in Fig. 4. In both cases the IMF B_Y -related effects contrary to anticipated
525 principles maximize at local night when the observatory is farthest apart from the Cusp region
526 where the IMF B_Y -related effects originate.

527 In a message 25 April 2014 to IAGA Executive Committee (EC) and PC index Task Force, the
528 index providers, Drs. O. Troshichev, AARI, and J. Matzka, DTU Space, wrote as a comment to the
529 objections against the methods defined in J&T2011 published in Stauning (2013b):

530 *“Dear colleagues,*
531 *We are thankful to all of you who contributed to the endorsement for the PC index.*
532 *We would like to remind that Dr. Stauning has expressed the same concern before the IAGA*
533 *meeting and we have responded to his criticism at the WG-5 Business meeting. Our arguments*
534 *were the following:*

535 *(i) We made allowance for Solar Wind sector structure effects while deriving QDC (Quiet Daily*
536 *Curve) as a level of reference to calculate the value of the polar cap magnetic disturbance. The*
537 *effect was exactly estimated for the daytime sector, where its value is maximal, and it was*
538 *roughly estimated in the nighttime sector, where its value is minimal. In principle, the effect could*
539 *be estimated exactly for any UT minute, but this would extremely complicate of the calculation*
540 *procedure and will not provide essential changes in the resulted PC index.”*

541 With this statement it appears that Drs. Troshichev and Matzka agree in the principle advocated in
542 Stauning (2013b, 2015) and in the present manuscript that the SWS effects should be maximal in
543 the daytime sector close to the Cusp region and minimal at night time. However, it has not been
544 possible to find the announced methods used for the “*roughly estimated*” nighttime SWS effects in
545 published literature. On the contrary, the methods published in J&T2011 or in Matzka (2014)
546 provide quite specific results which display maximal SWS effects at nighttime. Note also the
547 incorrect use of the term “quiet” in “*QDC (Quiet Daily Curve)*” for the median-based reference
548 level.

549 It is not, of course, questioned here that the IMF B_Y conditions significantly affect the polar
550 convection patterns and related magnetic variations. However, for the median-based reference level
551 construction, the assumption that slowly varying IMF B_Y levels would not affect geomagnetic
552 disturbance conditions has never been validated and may be incorrect in the complicated interplay
553 between the IMF B_Y - and B_Z - related effects. A further questionable feature in the reference level
554 derivation method is the implied assumption that SWS terms calculated from daily median values
555 could be applied to remove solar wind sector effects throughout the whole day disregarding the
556 variations in the IMF B_Y -related effects with the varying observatory position in the polar cap. The
557 real IMF B_Y -related SWS effects on the PC indices could even be opposite of the constructed
558 effects resulting from using reference level values derived by the median-based methods whether in
559 the post-event or in the real-time version.

560 The example PCN calculations displayed in Fig. 4 were based on the case presented in J&T2011
561 with a smoothed IMF B_Y value of 4 nT, which is not uncommon. Unjustified SWS contributions of
562 3-4 mV/m could be expected for the stronger cases (larger IMF B_Y). Such magnitudes are around
563 twice the onset level of around 2 mV/m for magnetic storm or substorm activity (Troshichev et al.,
564 2014), which definitely makes the IAGA-endorsed “final” PCN indices unsuitable for scientific
565 applications.

566 For the PCS indices, corresponding problems with the post-event reference levels may exist in spite
567 of the statement in p. 1492-1493 of J&T2011 that SWS effects are negligible at Vostok on the
568 Antarctic ice cap. It has not been possible to obtain a description of the present PCS calculation
569 methods from the index provider (AARI) or from the index publisher (ISGI) for further examination
570 of this issue.

571 For the real-time PCN and PCS indices, the excessive excursions in the cubic-spline extrapolated
572 reference levels may generate unfounded differences between near-real time and post-event index
573 values of more than 4 mV/m. Such excursions with magnitudes at magnetic storm levels make the
574 near-real time IAGA-recommended PC indices unreliable and thus unsuitable for Space Weather
575 monitoring and related research. Their strong vulnerability to intervals of incomplete data with the

576 maximum adverse effects appearing two days after the occurrence of data irregularities is an
 577 additional invalidating feature to be considered.

578 It has not been possible to obtain descriptions of the real-time PCN and PCS calculation methods
 579 from the index provider (AARI) or from the index publisher (ISGI). It has also not been possible to
 580 obtain archived recordings of near-real time PCN and PCS indices provided to the community
 581 through the AARI web portal <http://pcindex.org> and the ISGI web site <http://isgi.unistra.fr>.

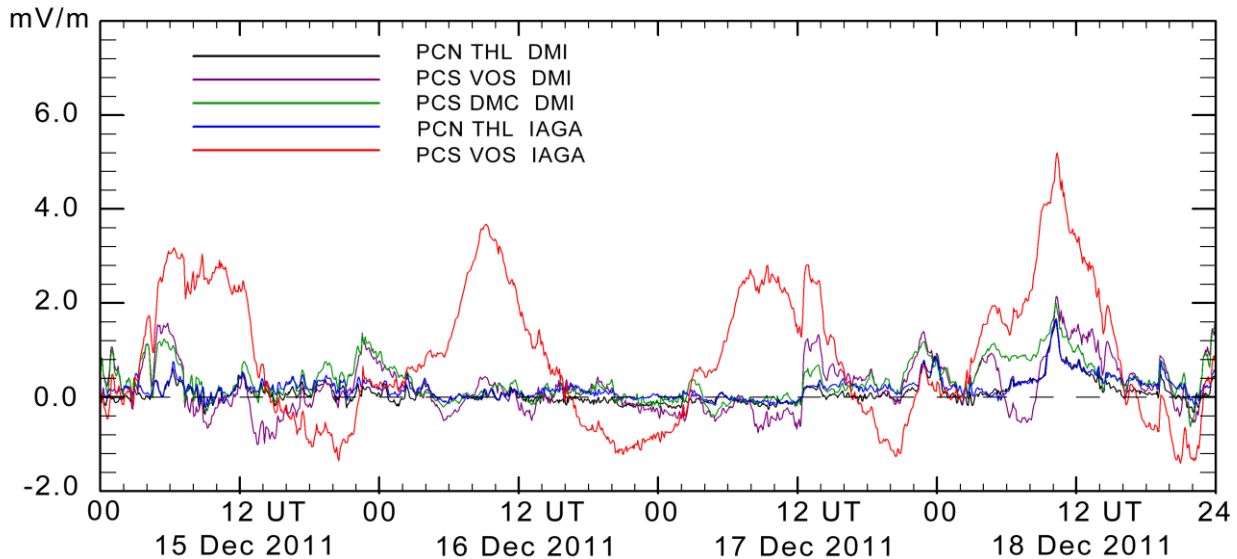
582 The concerns over the inconsistent index derivation methods and lack of documentation have been
 583 forwarded to IAGA Executive Committee, Index Task Force and Working Group representatives
 584 and to the PC index providers at AARI and DTU Space with suggestions for thorough analyses of
 585 PC index calculation methods. The specific concerns have not been responded to and the
 586 suggestions for further analyses of the index derivation methods have been rejected so far.

587

588 8. Irregular PCS excursions

589 The search for unjustified SWS effects in the PC index series has disclosed numerous examples of
 590 irregular unjustified PCS excursions. An example from a recent download of PCN and PCS data
 591 from 15-18 December 2011 is displayed in Fig. 11. Further examples are shown in an Appendix.

592 Fig 11 displays in addition corresponding PCN and PCS values derived by the DMI index
 593 procedure (Stauning, 2016). The display of PCS index values based on Vostok data is supplemented
 594 by PCS index values derived from Dome-C (DMC) magnetic data, which are of very good quality.
 595 The Vostok and Dome-C data generate nearly identical PCS values and indicate very low
 596 disturbance levels. The interval is very quiet (Kp values between 0 and 1) which is also evident
 597 from the PCN data in both versions.



598

599 **Figure 11.** Display of published PCN (blue line) and PCS (red) values from 15-18 December 2011. PCN
 600 (black) from Qaanaaq data, PCS from Vostok (magenta) and Dome-C (green) data derived by a different
 601 method (DMI, Stauning, 2016) have been added to the diagram.

602 It is easy to see that the published Vostok PCS data have unjustified daily variations between -1.5
 603 and up to +4.0 mV/m (a level indicative of strong magnetic storm conditions). The additional top of
 604 1 mV/m bringing the PCS value up to 5.0 mV/m at 11 UT on 18 December is probably a real event.
 605 The Vostok magnetic data supplied from INTERMAGNET are final values.

606 The excessive PCS variations are probably not caused by implementation of the SWS-related
607 reference level construction but may have resided in the PCS index values calculated at AARI
608 throughout the years and brought to attention now by the recent examination of PCS data for SWS
609 effects. The PCS index failure is mentioned here to underline the point that PC index series need
610 careful monitoring and evaluation of index quality, which is apparently not implemented.

611 Information on the problem in the PCS index series distributed from ISGI (<http://isgi.unistra.fr>) and
612 the AARI index web portal (<http://pcindex.org>) was published in Stauning (2018b) and also sent
613 directly to the index providers, and to ISGI and IAGA representatives in 2018. Their only reaction –
614 so far – has been to state that the published PCS index data are just provisional values to be applied
615 to scientific works at users own risk (communication from IAGA Executive Committee, 21 May
616 2018).

617

618 **Conclusions.**

619 - The Polar Cap indices in their real-time versions have the potential to become very important tools
620 for Space Weather monitoring and forecasts and in their final versions important for Space
621 Weather-related research. However, the presently published PCN and PCS index series are
622 considered invalid.

623 - The published series of (nominally) final PCN index values calculated by the methods endorsed
624 by IAGA may include unjustified contributions of up to 3-4 mV/m just due to the handling of IMF
625 B_Y -related solar wind sector effects in the reference level construction. An example case gave
626 unjustified contributions of up to 2.5 mV/m (magnetic storm level) to PCN index values. Such
627 unjustified contributions are considered to make the “final” PCN index series invalid.

628 - The series of near-real time PCN and PCS index values calculated by the methods endorsed by
629 IAGA may display considerable differences with respect to their corresponding post-event values.
630 An example case using the referenced calculation procedures to the letter gave differences of up to
631 2.8 mV/m for a moderate event. Further examples of calculations of effects have given differences
632 of more than 4 mV/m. At occasional downloads of near-real time index values and comparison to
633 later downloads of final values, differences of up to 3.7 mV/m have been documented in cases not
634 particularly extreme.

635 - The IAGA-endorsed near-real time index calculation method based on cubic spline extrapolation
636 of past median values is extremely vulnerable to irregularities in the data supply. An example of 12
637 hours of missing data gave unfounded excursions of up to 4 mV/m two days later. Such excursions
638 may falsely indicate (or hide) strong magnetic storm conditions and are considered to make the
639 IAGA-recommended near-real time indices highly unreliable and thus unsuitable for Space Weather
640 applications.

641 - The provisional PCS index series, which is not approved by IAGA but still made available from
642 ISGI and used in the scientific community, displays unexplained erroneous excursions of up to 4
643 mV/m in the recorded examples shown here. Final magnetic data were available for the index
644 examples and the IAGA-endorsed calculation methods were probably used. Similar or even larger
645 undetected excursions are possible. The example underlines the need for careful examination of
646 index quality in the published PC index series.

647 - It is suggested that IAGA should initiate a careful evaluation of present index series and index
648 derivation methods and ensure that full documentation of the presently applied index calculation
649 procedures is made available in agreement with its *Criteria for endorsement of indices by IAGA,*
650 *sec.2* (2009). Presently, there is no available documentation of present PCS index derivation
651 procedures or of the near-real time PCN and PCS calculation methods.

652 - On basis of the problems reported here, IAGA might consider encouraging developments of
 653 improved PC index calculation methods. Alternative more accurate and reliable methods are
 654 available.

655

656 **Data availability:**

657 Near real-time (prompt) PC index values and archived PCN and PCS index series derived by the
 658 IAGA-endorsed procedures are available through AARI and ISGI web sites. Archived PCN and
 659 PCS data used in the paper were downloaded from <http://pcindex.org> on 15 November 2019 unless
 660 otherwise noted. The web site, furthermore, holds PCN and PCS index coefficients. QDC and SWS
 661 values are not included. The web site includes the document “Polar Cap (PC) Index” (Troshichev,
 662 2011).

663 It is presently not known (in spite of requests) whether the near real-time PC index suppliers (AARI
 664 and ISGI) retain copies of the published values. If not available from the index suppliers, then
 665 values of occasionally downloaded values held by the author could be delivered, for instance, in
 666 their original (zip-encoded) formats to a data repository or included in a data supplement.

667 Geomagnetic data from Qaanaaq, Vostok, and Dome-C were supplied from the INTERMAGNET
 668 data service web portal at <http://intermagnet.org>.

669 The observatory in Qaanaaq is managed by the Danish Meteorological Institute, while the
 670 magnetometer there is operated by DTU Space, Denmark. The Vostok observatory is operated by
 671 the Arctic and Antarctic Research Institute in St. Petersburg, Russia. The Dome-C observatory is
 672 managed by Ecole et Observatoire des Sciences de la Terre (France) and Istituto Nazionale di
 673 Geofisica e Vulcanologia (Italy).

674 The “DMI” PC index version is documented in the report SR-16-22 (Stauning, 2016) available at
 675 the web site: http://www.dmi.dk/fileadmin/user_upload/Rapporter/TR/2016/SR-16-22-PCindex.pdf

676

677 **Acknowledgments.** The staffs at the observatories in Qaanaaq (Thule), Vostok, and Dome-C, and
 678 their supporting institutes are gratefully acknowledged for providing high-quality geomagnetic data
 679 for this study. The efficient provision of geomagnetic data from the INTERMAGNET data service
 680 centre, and the excellent performance of the PC index portals are greatly appreciated. The author
 681 gratefully acknowledges the good collaboration and many rewarding discussions in the past with
 682 Drs. O. A. Troshichev and A. S. Janzhura at the Arctic and Antarctic Research Institute in St.
 683 Petersburg, Russia.

684

685 **References**

686 Chun, F. K., Knipp, D. J., McHarg, M. G., Lu, G., Emery, B. A., Vennerstrøm, S., Troshichev, O.
 687 A. (1999), Polar cap index as a proxy for hemispheric Joule heating, *Geophys. Res. Lett.*, 26 ,
 688 1101-1104. <https://doi.org/10.1029/1999GL900196>

689 Chun, F.K., Knipp, D. J., McHarg, M. G., Lacey, J. R., Lu, G., and Emery, B. A. (2002), Joule
 690 heating patterns as a function of polar cap index, *J. Geophys. Res.*, 107 (A7),
 691 <https://doi.org/10.1029/2001JA000246> .

692 Iijima, T., Potemra, T.A. (1976). Field-aligned currents in the Cusp observed by Triad, *Journal of*
 693 *Geophysical Research*, 81, 5971-5979. <https://doi.org/10.1029/JA081i034p05971>

694 IAGA Resolution no. 3 (2013): <http://www.iaga-aiga.org/resolutions>.

- 695 IAGA Index endorsement criteria (2009):
696 https://www.ngdc.noaa.gov/IAGA/vdat/GeomagneticIndices/Criteria_for_Endorsement.pdf
- 697 Huang, C.-S. (2005), Variations of polar cap index in response to solar wind changes and
698 magnetospheric substorms, *J. Geophys. Res.*, 110, A01203,
699 <https://doi.org/10.1029/2004JA010616> .
- 700 Janzhura, A. S., Troshichev, O. A. (2008). Determination of the running quiet daily geomagnetic
701 variation. *Journal of Atmospheric and Solar-Terrestrial Physics*, 70, 962–972.
702 <https://doi.org/10.1016/j.jastp.2007.11.004> .
- 703 Janzhura, A. S., Troshichev, O. A. (2011). Identification of the IMF sector structure in near-real
704 time by ground magnetic data. *Annales Geophysicae*, 29, 1491-1500.
705 <https://doi.org/10.5194/angeo-29-1491-2011> .
- 706 Janzhura, A. S., Troshichev, O. A., Stauning, P. (2007). Unified PC indices: Relation to the isolated
707 magnetic substorms. *Journal of Geophysical Research*, 112, A09207.
708 <https://doi.org/10.1029/2006JA012132> .
- 709 Kan, J. R., Lee, L. C. (1979). Energy coupling function and solar wind-magnetosphere dynamo.
710 *Geophysical Research Letter*, 6 (7), 577– 580. <https://doi.org/10.1029/GL006i007p00577> .
- 711 Liou, K., Carbary, J. F., Newell, P. T., Meng, C. I., and Rasmussen, O. (2003). Correlation of
712 auroral power with the polar index, *J. Geophys. Res.*, 108 (A3), 1108,
713 <https://doi.org/10.1029/2002JA009556> .
- 714 Matzka, J. (2014). PC_index_description_main_document_incl_Appendix_A.pdf. Available at
715 DTU Space web portal: <ftp://ftp.space.dtu.dk/WDC/indices/pcn/>
- 716 Menvielle, M., Iyemori, T., Marchaudon, A., Nosé, M. 2010. Geomagnetic Indices. Ch.8 in: M.
717 Manda, M. Korte (eds), *Geomagnetic Observations and Models*, IAGA Special Sopron Book
718 Series 5, 2011. pp.183-228. https://doi.org/10.1007/978-90-481-9858-0_8
- 719 Nagatsuma T. (2002). Saturation of polar cap potential by intense solar wind electric fields,
720 *Geophys. Res. Lett.*, 29, (10), 621. <https://doi.org/10.1029/2001GL014202>
- 721 Nielsen, J. B. and Willer, A. N. (2019). Restructuring and harmonizing the code used to calculate
722 the Definitive Polar Cap Index, *Report from DTU Space*. <https://tinyurl.com/sx3g5t5>
- 723 Ridley A.J. and Kihn, E. A. (2004). Polar cap index comparisons with AMIE cross polar cap
724 potential, electric field, and polar cap area, *Geophys. Res. Lett.*, 31, L07801,
725 <https://doi.org/10.1029/2003GL019113> .
- 726 Stauning, P. (2011). Determination of the quiet daily geomagnetic variations for polar regions, *J.*
727 *Atmos. Solar-Terr. Phys.*, <https://doi.org/10.1016/j.jastp.2011.07.004> .
- 728 Stauning, P. (2012). The Polar Cap PC Indices: Relations to Solar Wind and Global Disturbances,
729 Exploring the Solar Wind, Marian Lazar (Ed.). *InTech Publ.*. ISBN: 978-953-51-0339-4.
730 <https://doi.org/10.5772/37359>
- 731 Stauning, P. (2013a). The Polar Cap index: A critical review of methods and a new approach, *J.*
732 *Geophys. Res. Space Physics*, 118, 5021-5038. <https://doi.org/10.1002/jgra.50462>
- 733 Stauning, P. (2013b). Comments on quiet daily variation derivation in “Identification of the IMF
734 sector structure in near-real time by ground magnetic data” by Janzhura and Troshichev (2011).
735 *Annales Geophysicae*, 31, 1221-1225. <https://doi.org/10.5194/angeo-31-1221-2013> .
- 736 Stauning, P. (2015). A critical note on the IAGA-endorsed Polar Cap index procedure: effects of
737 solar wind sector structure and reverse polar convection. *Annales Geophysicae*, 33, 1443-1455.
738 <https://doi.org/10.5194/angeo-33-1443-2015> .

- 739 Stauning, P. (2016). The Polar Cap (PC) Index.: Derivation Procedures and Quality Control. *DMI*
740 *Scientific Report SR-16-22*. Available at:
741 https://www.dmi.dk/fileadmin/user_upload/Rapporter/TR/2016/SR-16-22-PCindex.pdf .
- 742 Stauning, P. (2018a). A critical note on the IAGA-endorsed Polar Cap (PC) indices: excessive
743 excursions in the real-time index values. *Annales Geophysicae*, 36, 621–631.
744 <https://doi.org/10.5194/angeo-36-621-2018> .
- 745 Stauning, P. (2018b): Multi-station basis for Polar Cap (PC) indices: ensuring credibility and
746 operational reliability. *Journal of Space Weather and Space Climate*, 8, A07.
747 <https://doi.org/10.1051/swsc/2017036> .
- 748 Stauning P. 2013c. Power grid disturbances and polar cap index during geomagnetic storms, *J*
749 *Space Weather Space Clim.* 3: A22. <https://doi.org/10.1051/swsc/2013044> .
- 750 Stauning, P. (2018c). Reliable Polar Cap (PC) indices for space weather monitoring and forecast,
751 *Journal of Space Weather and Space Climate*, 8, A49. <https://doi.org/10.1051/swsc/2018031>
- 752 Stauning, P., Troshichev, O. A., and Janzhura, A. S. (2008). The Polar Cap (PC) index.: Relations
753 to solar wind parameters and global activity level, *J. Atmos. Solar-Terr. Phys.*,
754 <https://doi.org/10.1016/j.jastp.2008.09.028> .
- 755 Troshichev, O. A. (2011). Polar Cap (PC) Index. Available at: <http://pcindex.org> (see Supported
756 materials)
- Troshichev, O. A. and Andrezen, V. G. (1985). The relationship between interplanetary quantities
and magnetic activity in the southern polar cap. *Journal of Planetary and Space Science*, 33,
415-419. [https://doi.org/10.1016/0032-0633\(85\)90086-8](https://doi.org/10.1016/0032-0633(85)90086-8)
- 757 Troshichev, O. A. and Janzhura, A. S. (2012a). Physical implications of discrepancy between
758 summer and winter PC indices observed in the course of magnetospheric substorms. *Advances in*
759 *Space Research*, 50 (1), 77-84. <https://doi.org/10.1016/j.asr.2012.03.017>
- 760 Troshichev, O. A. and Janzhura, A. S. (2012b). Space Weather monitoring by ground-based means,
761 *Springer Praxis Books*. Heidelberg. <https://doi.org/10.1007/978-3-642-16803-1> .
- 762 Troshichev, A. O. and Lukianova, R. Y. (2002). Relation of PC index to the solar wind parameters
763 and substorm activity in time of magnetic storms, *J. Atmos. Solar-Terr. Phys.*, 64, 585.
764 [https://doi.org/10.1016/S1364-6826\(02\)00016-0](https://doi.org/10.1016/S1364-6826(02)00016-0) .
- 765 Troshichev, O. A., Sormakov, D. A. (2017). PC index as a proxy of the solar wind energy that
766 entered into the Magnetosphere: 3. Development of magnetic storms, *J. Atmos. Solar-Terr.*
767 *Phys.* <https://doi.org/10.1016/j.jastp.2017.10.012>
- Troshichev, O. A., Andrezen, V. G., Vennerstrøm, S., Friis-Christensen, E. (1988). Magnetic
activity in the polar cap – A new index. *Journal of Planetary and Space Sciences*, 36(11), 1095-
1102. [https://doi.org/10.1016/0032-0633\(88\)90063-3](https://doi.org/10.1016/0032-0633(88)90063-3)
- 768 Troshichev, O. A., Janzhura, A. S., Stauning, P. (2006). Unified PCN and PCS indices: method of
769 calculation, physical sense and dependence on the IMF azimuthal and northward components.
770 *Journal of Geophysical Research*, 111, A05208. <https://doi.org/10.1029/2005JA011402> . (note
771 correction in Troshichev et al., 2009)
- 772 Troshichev, O. A., Janzhura, A. S., Stauning, P. (2009). Correction to “Unified PCN and PCS
773 indices: Method of calculation, physical sense, and dependence on the IMF azimuthal and
774 northward components”, *Journal of Geophysical Research*, 114, A11202.
775 <https://doi.org/10.1029/2009JA014937> .

- 776 Troshichev, A. O., Lukianova, R. Y., Papitashvili, V. O., Rich, F. J. and Rasmussen, O. (2000).
777 Polar Cap index (PC) as a proxy for ionospheric electric field in the near-pole region, *Geophys.*
778 *Res. Lett.*, 27, 3809. <https://doi.org/10.1029/2000GL003756>
- 779 Troshichev, O. A. , Podorozhkina, N. A., Sormakov, D. A., Janzhura, A. S. (2014). PC index as a
780 proxy of the solar wind energy that entered into the magnetosphere: 1. Development of magnetic
781 substorms. *Journal of Geophysical Research, Space Physics*, 119.
782 <https://doi.org/10.1002/2014JA019940> .
- 783 Vassiliadis, D., V. Angelopoulos, D. N. Baker, A. J. Klimas (1996), The relation between the
784 northern polar cap and auroral electrojet geomagnetic indices in the wintertime, *Geophys. Res.*
785 *Lett.*, 23, 2781. <https://doi.org/10.1029/96GL02575> .
- 786 Vennerstrøm, S. (1991). The geomagnetic activity index PC, PhD Thesis, Scientific Report 91-3,
787 Danish Meteorological Institute, 105 pp.
788 https://www.dmi.dk/fileadmin/user_upload/Rapporter/SR/1991/sr91-3.pdf
- 789 Vennerstrøm, S., Friis-Christensen, E., Troshichev, O. A., Andrezen, V. G. (1991). Comparison
790 between the polar cap index PC and the auroral electrojet indices AE, AL and AU, *J. Geophys.*
791 *Res.*, 96, 101. <https://doi.org/10.1029/90JA01975>
- 792 Wilhelm, J., Friis-Christensen, E., Potemra, T. A. (1972). The relationship between ionospheric
793 and field-aligned currents in the dayside cusp, *J. Geophys. Res.* 83, 5586.
794 <https://doi.org/10.1029/JA083iA12p05586>

795

Funding:

797 No external funding was involved in this work.

798

Conflict of interest:

800 I have no conflict of interest

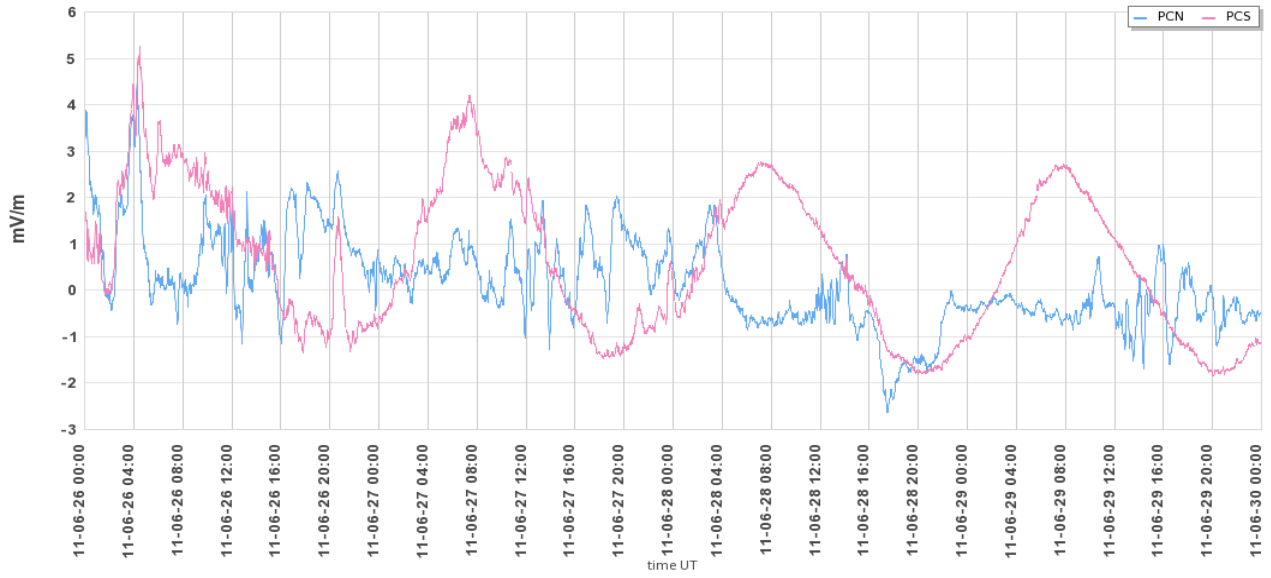
801

Appendix (for the review process only).

803 Further PCN/PCS examples downloaded from the graphical output of <http://pcindex.org> on 15
804 November 2019. Examples with quiet conditions have been selected as the unjustified PCS
805 excursions are then easy to detect.

806

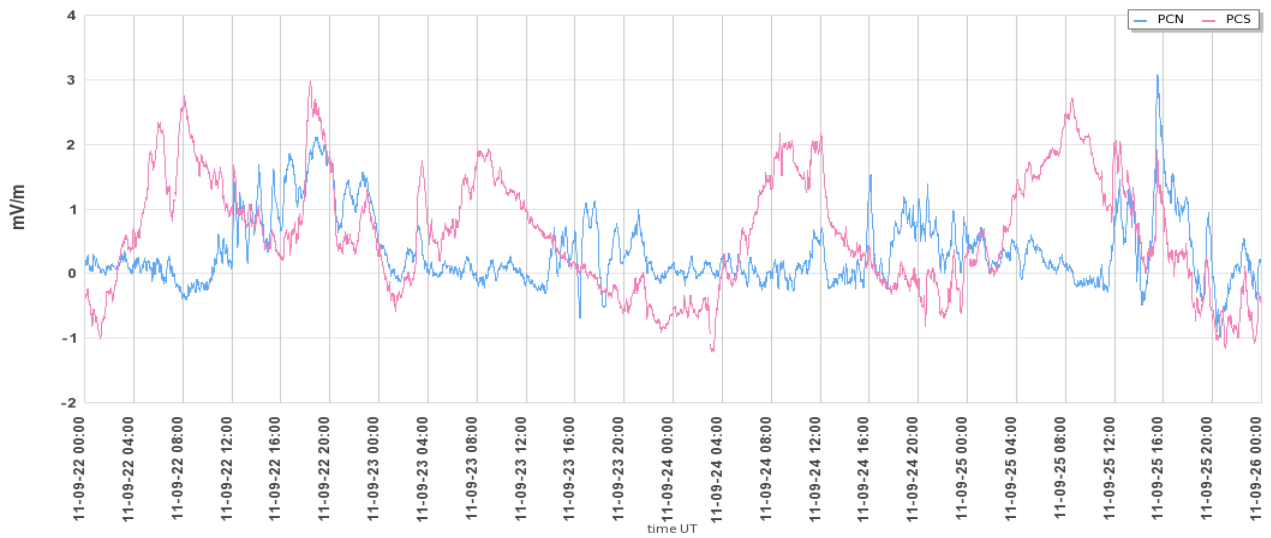
807 **1.** PCN/PCS 26-30 June 2011



808

809

810 **2. PCN/PCS 23-26 September 2011**



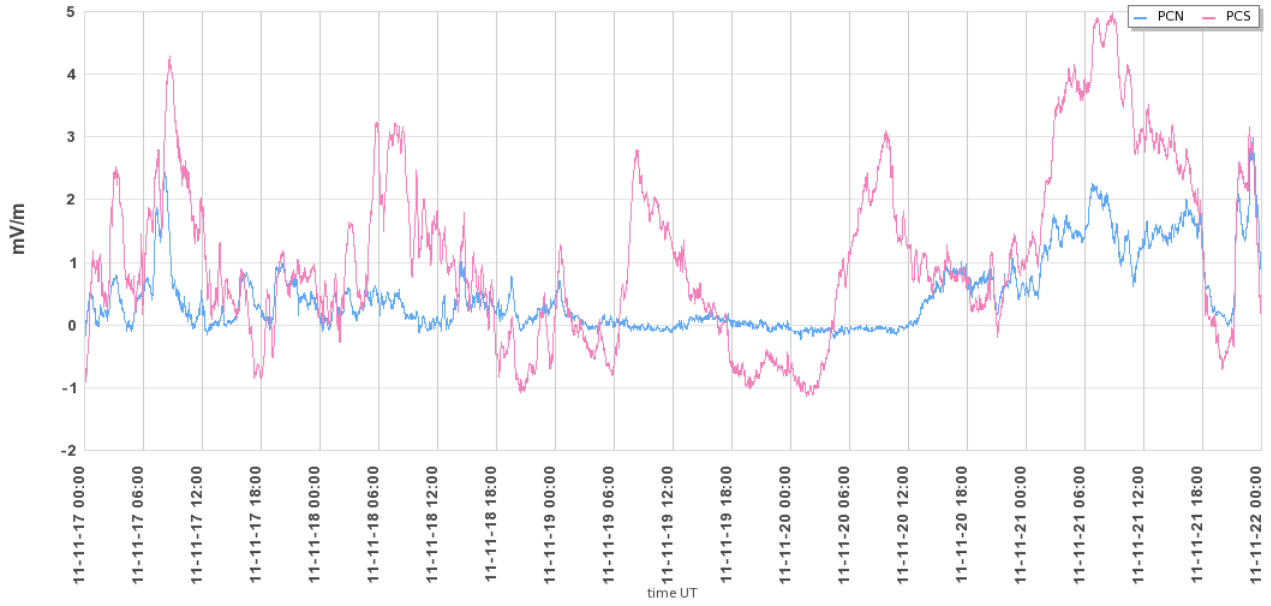
811

812

813

814 **3. PCN/PCS 17-21 November 2011**

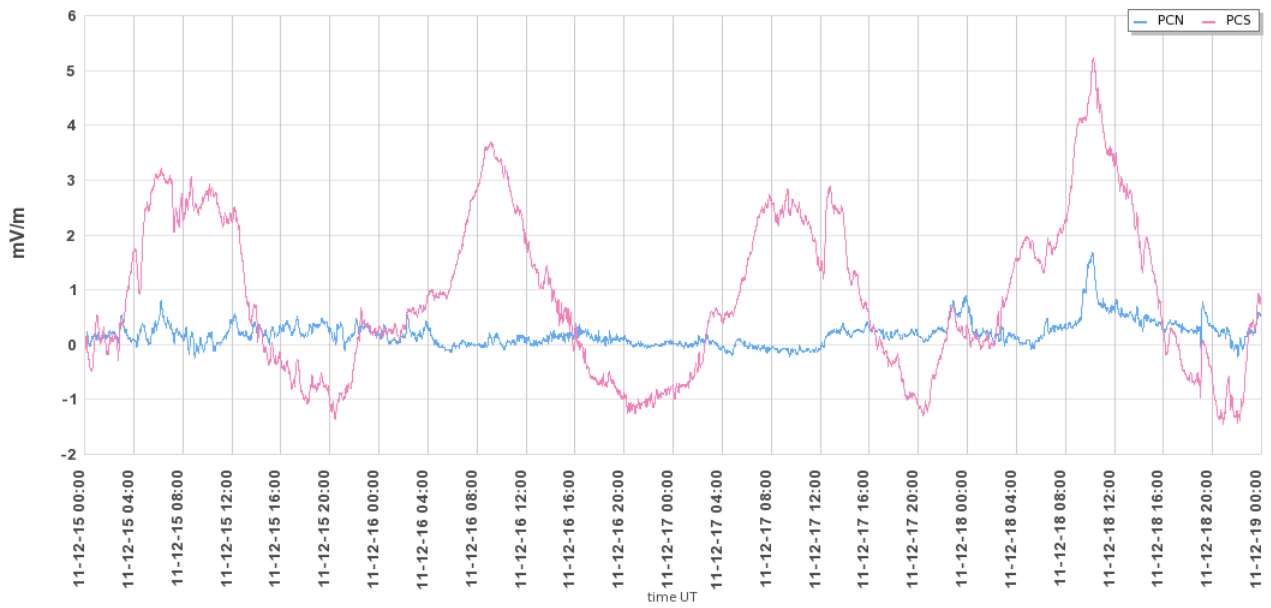
815



816

817

818 4. PCN/PCS 15-18 December 2011 (also in Fig.4)



819